J. exp. Biol. ***174****, 45–64 (1993)*
Printed in Great Britain © The Company of Biologists Limited 1993

UNSTEADY AERODYNAMIC PERFORMANCE OF MODEL WINGS AT LOW REYNOLDS NUMBERS

BY MICHAEL H. DICKINSON* AND KARL G. GÖTZ

Max Planck Institute für Biologische Kybernetik, Spemannstrasse 38, D7400 Tübingen 1, FRG

Accepted 17 August 1992

Summary

The synthesis of a comprehensive theory of force production in insect flight is hindered in part by the lack of precise knowledge of unsteady forces produced by wings. Data are especially sparse in the intermediate Reynolds number regime ($10<Re<1000$) appropriate for the flight of small insects. This paper attempts to fill this deficit by quantifying the time-dependence of aerodynamic forces for a simple yet important motion, rapid acceleration from rest to a constant velocity at a fixed angle of attack. The study couples the measurement of lift and drag on a two-dimensional model with simultaneous flow visualization. The results of these experiments are summarized below.

1. At angles of attack below 13.5°, there was virtually no evidence of a delay in the generation of lift, in contrast to similar studies made at higher Reynolds numbers.

2. At angles of attack above 13.5°, impulsive movement resulted in the production of a leading edge vortex that stayed attached to the wing for the first 2 chord lengths of travel, resulting in an 80% increase in lift compared to the performance measured 5 chord lengths later. It is argued that this increase is due to the process of *detached vortex lift*, analogous to the method of force production in delta-wing aircraft.

3. As the initial leading edge vortex is shed from the wing, a second vortex of opposite vorticity develops from the trailing edge of the wing, correlating with a decrease in lift production. This pattern of alternating leading and trailing edge vortices generates a von Karman street, which is stable for at least 7.5 chord lengths of travel.

4. Throughout the first 7.5 chords of travel the model wing exhibits a broad lift plateau at angles of attack up to 54°, which is not significantly altered by the addition of wing camber or surface projections.

5. Taken together, these results indicate how the unsteady process of vortex generation at large angles of attack might contribute to the production of aerodynamic forces in insect flight. Because the fly wing typically moves only 2–4 chord lengths each half-stroke, the complex dynamic behavior of impulsively started wing profiles is more appropriate for models of insect flight than are steady-state approximations.

Introduction

Insects were the first creatures to develop flight and remain in many ways unsurpassed

*Permanent address: Department of Organismal Biology and Anatomy, The University of Chicago, 1025 E. 57th Street, Chicago, IL 60637, USA.

Key words: insect, flight, wings, aerodynamics, vortex lift.

in aerodynamic wizardry. Yet because of the kinematic complexity of wing movements, the analysis of force production in insects pushes the limits of our understanding of aerodynamic mechanisms. Early attempts to explain force production during insect flight, pioneered by Weis-Fogh and Jensen, relied on the 'quasi-steady state' model, which assumes that steady-state forces are produced by the wing at each instantaneous position throughout a full stroke cycle (Jensen, 1956; Weis-Fogh, 1973). Thus, the aerodynamic forces produced by a given wing profile were assumed to depend solely on the angle of attack, the geometry of the wing and relative fluid velocity, while all time-dependent characteristics of force generation were ignored. Ellington (1984*a*) in a comprehensive review rejected the quasi-steady state theory on the basis that the predicted lift coefficients of wings necessary to generate lift according to the steady-state theory are higher than those actually measured. Subsequently other authors have provided additional evidence on the limitations of the quasi-steady theory based upon this method (Ennos, 1989; Dudley and Ellington, 1990; Zanker and Götz, 1990). Further, the fundamental assumption of the quasi-steady state model has been challenged on basic theoretical grounds by invoking the mathematical work of Wagner (1925), who calculated that maximal lift is produced only after several chord lengths of travel (Ellington, 1984*b*). The Wagner effect was demonstrated experimentally by Walker (1931), at a Reynolds number of 140000, but has never been subsequently examined at an intermediate Reynolds number range that is more appropriate for the flight of insects.

As described above, the rejection of the quasi-steady state theory has heretofore been based on internal inconsistencies. More rare, however, are direct experimental investigations of unsteady mechanisms, with the noted exception of the 'clap and peel' behavior of *Drosophila* and *Encarsia* (Weis-Fogh, 1973; Ellington, 1975; Götz, 1987), which has been analyzed using physical models (Bennett, 1977; Maxworthy, 1979; Spedding and Maxworthy, 1986) and received much theoretical attention (Lighthill, 1973; Maxworthy, 1979; Ellington, 1980, 1984*b*). Unsteady flows have also been visualized around model (Savage *et al.* 1979) and actual (Somps and Luttges, 1985) dragonfly wings operating at higher Reynolds numbers. Several other proposed, but less well studied, unsteady mechanisms have been reviewed by Nachtigall (1979), Maxworthy (1981) and Ellington (1984*b*).

The purpose of this analysis is not to drive yet another nail into the quasi-steady state coffin, but rather to characterize the time-dependence of forces produced by impulsively moved wings and thereby expand the knowledge of unsteady mechanisms that might be employed by insects during flight. In particular, we are concerned with the time history of two processes: the generation of lift and the onset of stall. Although lift and stall require only a few chord lengths of travel to approach their steady-state values, this range typically exceeds the movements of a fly wing during a single half-stroke. Further, because of the propensity for the creation of a von Karman street in the range of Reynolds numbers relevant for insect flight (Schlichting, 1979), the concept of 'steady-state' lift and stall may be entirely inappropriate even after an infinite number of chord lengths of travel. We have concentrated our study on a small, yet critical, range of Reynolds numbers appropriate for flies of the genus *Drosophila* and other small insects. These

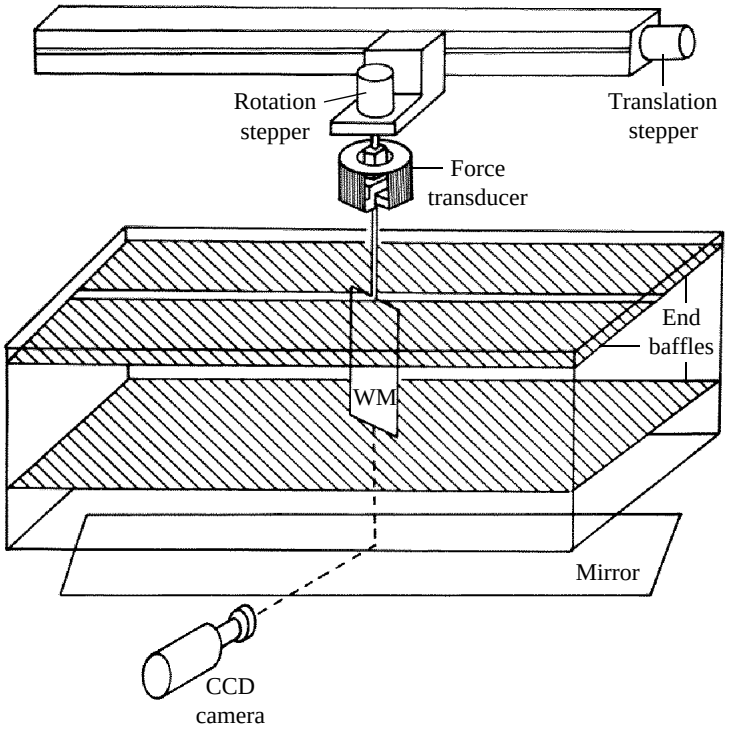

Fig. 1. Experimental apparatus for measurement of aerodynamic forces during acceleration of a wing to constant velocity starting from rest. The translation of a sled holding the two-dimensional force transducer and the wing model (WM) was accomplished by using an Isel (Eiterfeld, FRG) linear translator, manufactured for machine shop use. The device consisted of a threaded rod driven by a computer-operated stepper motor. A second stepper motor was attached to the sled, allowing programmed changes in angle of attack. The force transducer consisted of two pairs of phosphor-bronze shims mounted with four 350 Ω foil strain gauges wired in full bridge configuration. The brass rod holding the wing model was oriented so that the transducer measured forces perpendicular and parallel to the axis of the section, regardless of angle of attack. Lift and drag forces were subsequently recovered through trigonometric transformation. The wing model was submerged in the 200l aquarium filled with 54% sucrose solution. The aquarium contained a set of acrylic baffles, placed just above and beneath the 15cm model, in order to limit spanwise flow. A long mirror was placed underneath the aquarium at 45° to allow observation of fluid movement. Flow visualization was achieved by mixing the sucrose solution with fine aluminium shavings illuminated by a sheet of red light intersecting the model wing at its mid-section.

results will be used to determine whether unsteady processes could be important for the generation of flight forces in these small insects.

Materials and methods

Flow tank, model wings and force measurement

The basic experimental apparatus is shown schematically in Fig. 1. All experiments

employed a 1mm thick aluminium wing section with a 5cm chord and 15cm length. The wings were bluntly rounded on the leading edge and sharply tapered at the trailing edge. The test chamber consisted of a 100cm×40cm×60cm glass aquarium filled with 54% sucrose solution. The aquarium was fitted with two edge baffles placed within 5mm of the upper and lower edges of the profile in order to limit spanwise flow. At room temperature, this solution has a predicted kinematic viscosity of 0.197stokes ($cm^2\,s^{-1}$). However, owing to temperature variation, evaporation and inaccuracies inherent in filling a 200l aquarium, the viscosity was calculated daily by measuring the terminal velocity of a 0.2mm steel sphere and employing Stokes' Law. Measured kinematic velocities ranged from 0.25 to 0.22stokes.

The forces on the wing model were measured using a two-dimensional force transducer consisting of orthogonal sets of parallel phosphor-bronze plates. The force platform was designed to minimize cross-talk, while allowing similar mechanical sensitivity and inertial characteristics on both axes. Foil strain gauges (350 Ω, HBM) were mounted on both sides of each plate and wired in full bridge configuration (four for each axis). The sensitivities of the two transducer axes with 10V excitation were 692 and 738 NV^{-1}. Cross-talk between channels was calculated in static measurements to be no greater than 0.45%. The wing was fixed to the underside of the force transducer so that one channel measured forces parallel to the flat surface of the profile and the other channel measured forces perpendicular to the profile. These forces were then used to calculate the lift and drag components through simple trigonometric functions of the angle of attack. The force records were filtered on line using a two-pole Butterworth low-pass filter with a 5Hz cut-off setting. Following the inertial transients, the fastest oscillations in the force records produced by translation of the wing model were estimated to have a spatial frequency of about 0.05cyclescm^{-1}. At the chosen filter settings such a signal would be distorted by phase lag of 3–8°, depending upon the translation velocity (Tietze and Schenk, 1990). These predicted phase lags are rather small and have been ignored in all subsequent analysis. Following filtration, the analog signals were digitized, averaged (four traces for each angle of attack) and stored on disk for subsequent analysis. The data were subsequently filtered digitally, with cut-offs ranging from 1 to 5 Hz, depending upon the velocity of the wing model. Symmetrical digital filters were used so as not to introduce any additional phase delays (Marmarelis and Marmarelis, 1978).

The wing was mounted vertically to the underside of the force platform using a 7.5cm long, 8mm diameter brass sting. The force transducer and wing were attached to the movable sled of an automated milling device (Isel), driven by two computer-operated four-phase stepper motors that permitted translation and rotation of the wing platform through the sucrose tank. Each command pulse from the power amplifier resulted in 0.125mm of horizontal translation. In all experiments the wing was moved impulsively from rest for 37.5cm (7.5 chord lengths). In most trials, the transition from rest to fixed velocity was accomplished by a constant acceleration of 62.5cm s^{-2}. We used a sufficiently powerful amplifier (Isle C142), so that each command pulse (at rates up to 10000 pulses s^{-1}) was faithfully followed by the stepper motors.

Each experimental run consisted of 23 different angles of attack from −9 to 90° in 4.5° increments. We accomplished a spread of Reynolds number values by varying the

translational speed from 4 to 12cm s^{-1}, while leaving kinematic viscosity and chord length constant.

Inertial subtraction

Several masses contributed to the production of force transients measured by the transducer during acceleration of the wing. The contribution of the transducer and sting mass could be measured directly by repeating each trial after removal of the aluminium profile. These force records were then subtracted from the trajectories measured with the wing attached. While the profile itself contributed little mass to the system (assessed by testing an equivalent cylindrical mass to the end of the sting), the added mass of fluid around the wing generated large inertial transients during acceleration. These added mass contributions, which vary with angle of attack, could not be easily separated from aerodynamic forces. However, in all the subsequent analyses, the earliest measurements of lift and drag transients were taken a full chord length after steady-state velocity had been reached. This is equivalent to approximately four ramp times after the acceleration drops to zero. Further, we performed control experiments in which four different accelerations were used to reach the final velocity (31.25, 62.5, 93.75 and 125cm s^{-2}). Varying the initial acceleration altered the width and peak of the initial transient, but had no effect on the subsequent force record. Thus, we are satisfied that the aerodynamic forces discussed here were not contaminated by the transient inertial forces.

Calculation of force coefficients

Measurements of lift and drag coefficients [$C_L(t)$ and $D_L(t)$] were based on the standard formula for airfoils:

$$C_L(t) = 2L(t)(\rho S U^2)^{-1}, \quad (1)$$

$$C_D(t) = 2D(t)(\rho S U^2)^{-1}, \quad (2)$$

where ρ is fluid density, S is the plan area and U is the final velocity of the profile. The only unusual modification is the treatment of lift and drag forces [$L(t)$ and $D(t)$], as well as their respective coefficients as functions of time. It will be useful to compare the measured values with simple steady-state predictions. At small angles of attack in uniform flow, the expected lift coefficient of a planar wing is approximated by (Keuthe and Chow, 1986):

$$C_L = 2\pi \sin\alpha, \quad (3)$$

where α is the aerodynamic angle of attack.

The drag on an airfoil parallel to flow is typically separated into three components: pressure drag, skin friction and induced drag. At small angles of attack and with end baffles limiting spanwise flow, the pressure and induced drag terms can be ignored, resulting in the relationship (Schlichting, 1979):

$$C_D = 2.66 Re^{-0.5}, \quad (4)$$

where Re is the Reynolds number. In the case of a two-dimensional flat plate normal to flow, the drag may be approximated by the relationship (Ellington, 1991):

$$C_D = 1.95 + 50/Re\,. \quad (5)$$

Comparisons of the theoretical predictions of equations 4 and 5 with measured values of C_D provide useful tests of the two-dimensional nature of flow around the model wings in our apparatus.

Flow visualization

In order to correlate the direct force measurements with fluid movement during translation of the profiles, we suspended aluminium particles in the sucrose solution. This fine dust was illuminated with red light originating from sets of light pipes facing all four surfaces of the tank. The sides of the tank were covered with opaque black contact paper except for a 1cm slit, producing a horizontal plane of red light which sliced the wing through its mid-section. The illuminated plane of fluid was visualized with a CCD camera (Philips) and recorded on video tape. The lift and drag signals were fed into two voltage control oscillators and recorded on the left and right audio channels of the tape recorder. It was then possible to watch the flows while 'hearing' the orthogonal forces on the wing. This arrangement was extremely useful in qualitatively analyzing the role of fluid vortices in force production.

Results

Time-dependence of force production

Examples of C_L and C_D plotted as functions of chord lengths traveled are shown in Fig. 2 for 23 angles of attack between −9 and 90° (Reynolds number 192). The inertial force resulting from the rapid acceleration of the wing model and added mass can be clearly seen as a sharp transient force peak at the start of each trace which decays after about 0.7 chord lengths of travel. At angles of attack ranging from −9 to 18°, both force coefficients reach their steady-state values by the end of one chord length of travel and remain constant throughout the course of translation. As expected from the Wagner effect, there is a slight sluggishness in the growth of the lift at low angles of attack. However, the magnitude of this effect is rather small and C_L grows little after 2 chords of movement. Above 13.5°, the time-dependence of force generation changes quite dramatically, as a broad bump in C_L appears, peaking after about 2 chord lengths. This transient bump becomes stronger at increasing angles of attack and gives way by 27° to a clear pattern of oscillation. The magnitude of these oscillations is more substantial in the time history of C_L than in that of C_D, at angles of attack less than 31.5°.

The time history of the aerodynamic force coefficients correlated with the pattern of vortex shedding by the profile. Fig. 3 shows video images for the first five chord lengths of travel for 9 and 45° angles of attack. At 9°, a thin separation bubble, barely visible in the video images, quickly forms on the upper surface of the airfoil and remains stable throughout the duration of translation. This stability of flow correlates with the resulting force, which is virtually constant after the first chord length of travel. In contrast, at an angle of attack of 45°, a vortex rapidly develops on the leading edge of the wing. The vortex is quite large, with a diameter that is roughly equivalent to the chord length of the

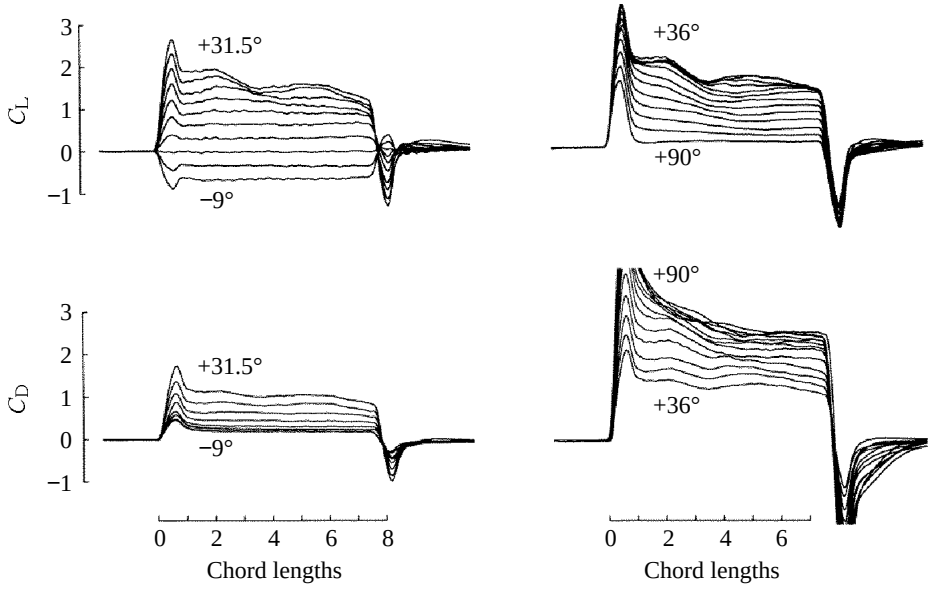

Fig. 2. Aerodynamic force coefficients display strong time dependency at angles of attack above 13.5˚. This figure shows the C_L and C_D trajectories at 23 angles of attack between −9 and 31.5˚ (left column) and 36 and 90˚ (right column) in 4.5˚ steps. Significant unsteady behavior can be clearly seen at angles of attack greater than 13.5˚. The Reynolds number was 192, based on the steady-state velocity of $10\,cm\,s^{-1}$, achieved through an initial constant acceleration of $62.5\,cm\,s^{-2}$. The sharp peaks at the start and end of each trace result from the inertial forces generated during rapid acceleration and deceleration of the wing profile. The inertial forces due to the mass of the force transducer and sting have been subtracted. Each trace represents the average of four trials at the same angle of attack. Similar sets of traces make up the basic raw data for each of the Reynolds number values shown in Fig. 4.

wing. The height of the vortex is much greater than those generated by surface corrugations (Rees, 1975; Newman *et al.* 1977), which are purported to increase effective wing camber. During the time of maximal lift production (2–2.5 chord lengths), the vortex remains on the upper surface of the wing. After about 4 chord lengths of travel, the vortex becomes extended rearward and is eventually shed from the profile. As this

Fig. 3. Flow patterns during translation of model wings. (A) Single-frame video images are shown for the first 4 chord lengths (C_L) of travel at 9˚ (left) and 45˚ (right) angles of attack (*Re*=192). The abbreviation C_L used in this figure should not be confused with the abbreviation C_L used for lift coefficient elsewhere in the manuscript. At 9˚ the pattern of flow is stable throughout translation, which correlates with the lift and drag measurements shown in Fig. 2. At 45˚ the pattern of flow is unsteady, displaying an alternating pattern of vortex generation from the leading and trailing edges. (B) A higher-resolution image of the flow after 2.5 chord lengths of travel, near the time of maximal lift production. At 45˚, this point of lift augmentation correlates with the presence of a large leading edge vortex attached to the upper surface of the profile. Note that fluid is moving tangentially forward from the leading edge of the wing in a pattern analogous to the Kutta condition.

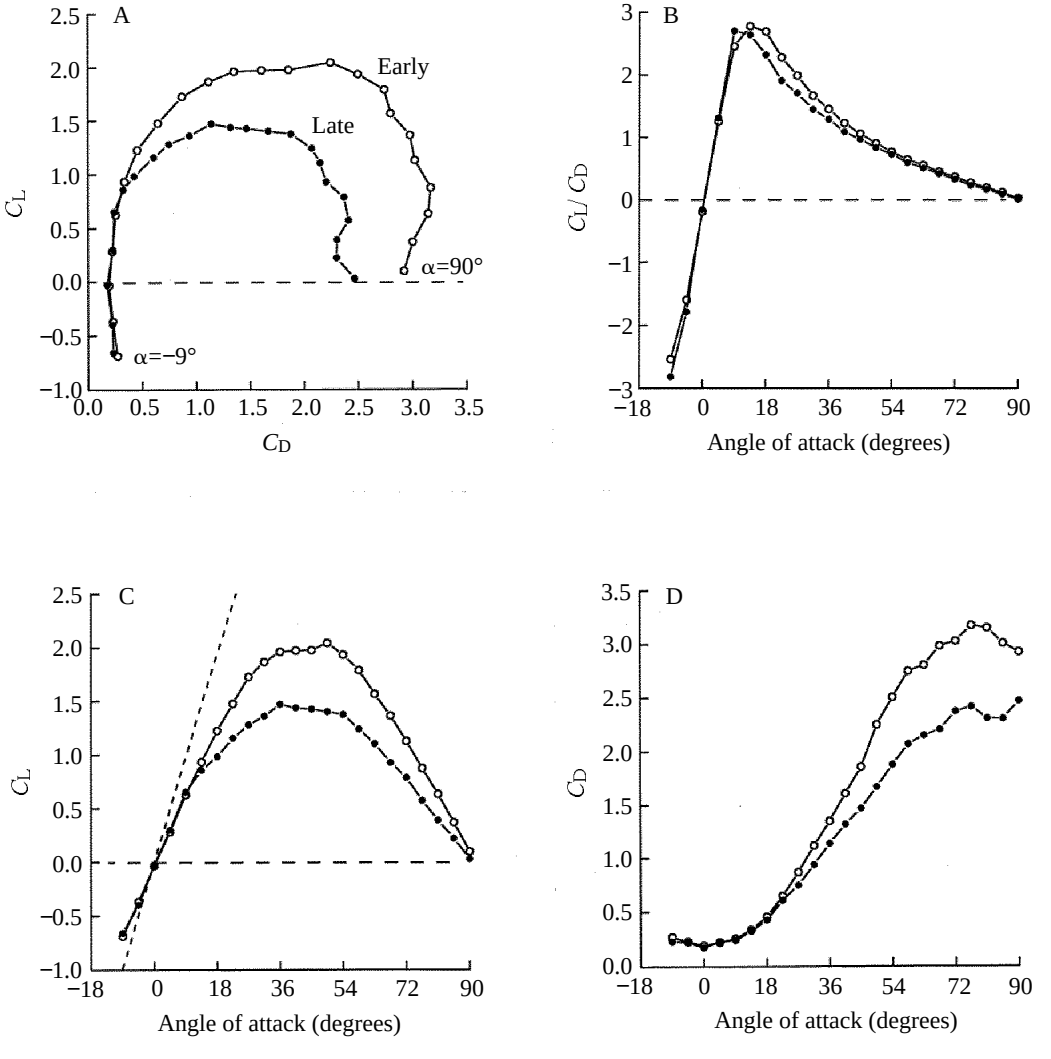

Fig. 4. Aerodynamic performance of wing model is enhanced early in translation. (A) Conventional polar plot of lift and drag coefficients parameterized by angle of attack (*Re*=192). Data are given for all 23angles of attack (α) between −9 and 90˚ in 4.5˚ steps. Open circles and filled circles show the data for early (2 chords) and late (7 chords) points, respectively. This convention is followed in B, C and D. (B) The ratio of lift to drag coefficients at early and late points plotted as a function of angle of attack. The maximum C_L/C_D ratio is similar at both the 2 and 7 chord positions, but peaks at a lower angle of attack (near 9˚) late in translation. Above 13.5˚ the C_L/C_D ratio is significantly higher after two chords travelled than after seven. (C) Early and late lift coefficients plotted against angle of attack. The dotted line in this panel indicates the $2\pi\sin\alpha$ dependence predicted from steady-state thin airfoil theory (equation 3). (D) Early and late drag coefficients plotted against angle of attack.

leading edge vortex is being shed, a vortex of opposite sign develops on the trailing edge. This alternating pattern continues, resulting in a von Karman street, whose time history is tightly correlated with the oscillations of the force records.

A conventional polar plot of the two force coefficients parameterized by angle of attack is shown in Fig. 4A. Two polar functions are shown, corresponding to the instantaneous values measured after 2 and 7 chord lengths of travel. For convenience, we term these data the 'early' and 'late' values, respectively. The early and late performance of the wing model is very similar at angles of attack below 13.5°. Above 13.5°, the polar diagrams indicate a significant deviation between the early and late values of C_L and C_D. Whereas the late value of C_L reaches a plateau of 1.5 by 36°, the early values exceed 2.0. A sharp stall is absent at both early and late time points and the model generates a broad lift plateau between 27 and 54°. The slopes of the two polar diagrams are different within the plateau, however, as the early C_L continues to grow gradually until 54°, whereas the late values of C_L show a slight decline within this range. Above 54°, both the early and late polar curves display a precipitous decline, as C_L falls towards zero.

One way of comparing the performance of the airfoil at early and late stages in translation is to compare the ratio of lift and drag coefficients (C_L/C_D) as a function of angle of attack, as shown in Fig. 4B. There is little difference in the maximum C_L/C_D ratios for the early and late time points. However, at angles of attack above 13.5°, the performance of the airfoil is significantly better early in translation. At low angles of attack (between 0 and 13.5°), the ratio is actually higher late in translation, which presumably reflects the influence of the Wagner effect causing a slight delay in the generation of lift. However, as argued by Vogel (1981), the production of lift *per se* and not the lift to drag ratio, may be a more important parameter of wing performance at low Reynolds number. Thus, the greatest benefit available from the unsteady flow may be the large augmentation in lift, and not the increase in the lift to drag ratio at large angles of attack.

Direct plots of the force coefficients against angle of attack are shown in Fig. 4C,D. The data for C_L are also compared to the predictions of thin airfoil theory (equation 3). Clearly, this theoretical prediction, which requires the assumption of inviscid flow, gives an overestimation of C_L. The measured value of $dC_L/d\alpha$ at low angles of attack was 4.5, compared to a theoretical value of 2π. Fig. 4C also shows a small but reproducible 'stutter' in the growth of the late C_L with angle of attack between 9 and 13.5°. This stutter is reminiscent of steady-state *thin airfoil stall* characterized by McCullough and Galt (1951) and is manifest as a large notch in Nachtigall's (1977) polar plots of *Tipula* wings. This phenomena arises from the sudden transformation of a short leading-edge separation bubble into a longer less stable bubble and probably indicates the breakdown of a thin separation bubble that was seen on the upper surface of the airfoil at angles of attack below 13.5°. However, thin airfoil stall is a steady-state phenomenon and the analogy with the performance of these flat plate models at low Reynolds numbers must be made cautiously. On conventional airfoils at higher speeds, the long separation bubble that develops above the stutter angle remains low in height, but continues to grow in length as the reattachment point creeps back towards the trailing edge with increasing angle of attack (Tani, 1961). In the case of the impulsively started model wings, it appears that the

separation bubble does not remain flat against the wing surface. Rather, it quickly enlarges into a large leading edge vortex that will eventually become the second element in a von Karman street.

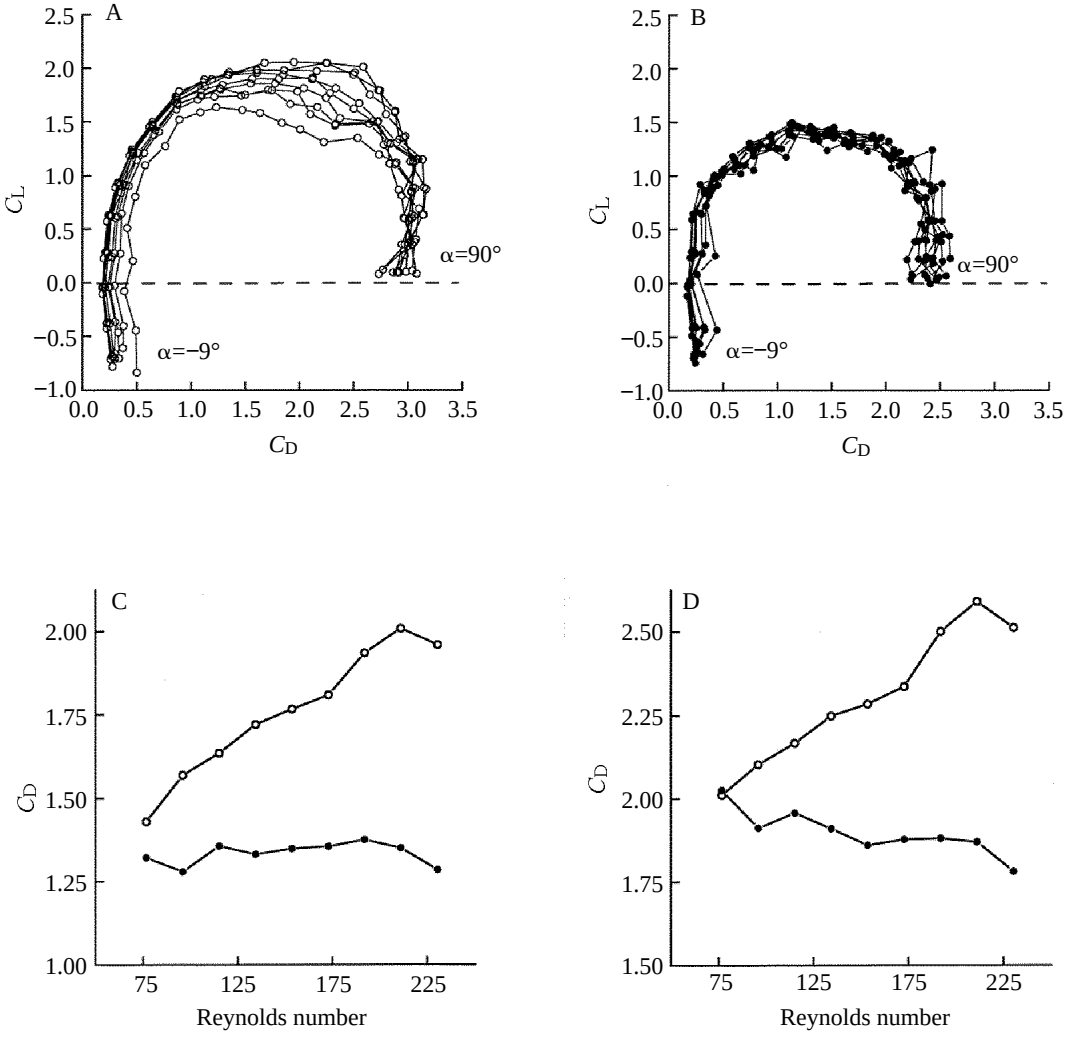

Fig. 5. The transient augmentation of force coefficient is strongly dependent on Reynolds number. Data are shown for nine (A,B) different Reynolds numbers between 79 and 236 in steps of 19. The polar plots calculated after 2 and 7 chord lengths of travel are shown in A and B, respectively. The change in Reynolds number has little affect on the late polar plots but a significant effect on the early polar plots, especially at angles of attack above 27˚. (C) The lift coefficients at 54˚ for early (open circles) and late (filled circles) times are plotted as a function of Reynolds number. Only the early C_L values show a dependence on Reynolds number within this range. (D) Same plot as in C, but showing C_D. As expected for steady-state forces, there is a slight decrease in the late values of C_D with increasing Reynolds number. However, within this same range the early C_D values grow with increasing contribution of inertial forces.

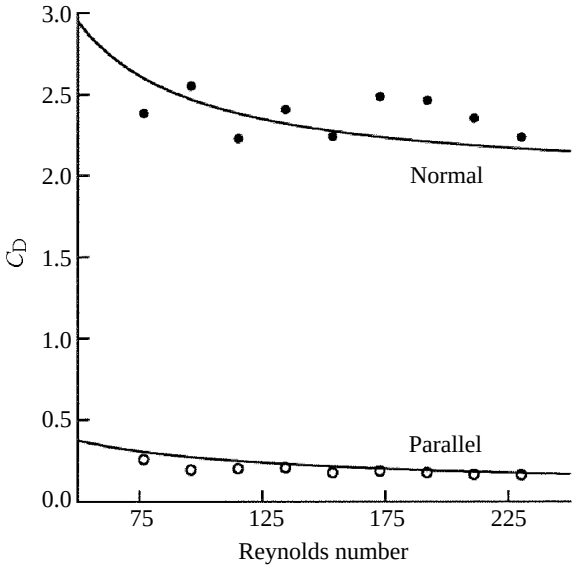

Fig. 6. The measured dependence of C_D on Reynolds number closely fits theoretical predictions for a wing of infinite span. The measured values of C_D late in translation are plotted as a function of Reynolds number at 0˚ (open circles) and 90˚ (filled circles) angles of attack. These data correspond to the 0 and 90˚ points of the polar diagrams in Fig. 5B. The solid curves show the predictions of equations 4 and 5, which are based on the assumptions of two-dimensional flow.

The effect of Reynolds number on unsteady forces

Similar data to those shown in Figs 2–4 were generated for a linear series of Reynolds numbers appropriate for the wing kinematics of drosophilid flies. Although this is a rather small range, the performance of the model wing did change significantly within this domain. Fig. 5A,B shows the transient and steady-state polar plots measured at nine different Reynolds numbers between 79 and 236. While increasing Reynolds number has very little bearing on the shape of the late polar plots, the effect on the early force coefficients is striking, particularly at high angles of attack. This Reynolds number effect is greatest at angles of attack between 45 and 54˚, producing an ‘aneurysm’ in the late polar plots within this range. This trend is examined more closely in Fig. 5C,D, which plots the values of C_L and C_D at 54˚ as a function of Reynolds number. Changes in the ratio of viscous to inertial forces has little effect on the late force coefficients, except for a slight decrease in C_D with increasing Reynolds number, which is the expected trend from steady-state measures of drag on bluff bodies. In contrast, the values of both C_L and C_D measured early in translation both *increase* with increasing Reynolds number. Thus, the dependence of the force coefficients on Reynolds number is entirely different at the early and late points in translation, separated by a mere 5 chord lengths of travel. The early augmentation of wing performance decreases as the contribution of viscous forces becomes greater. This is expected of an unsteady mechanism that depends on the

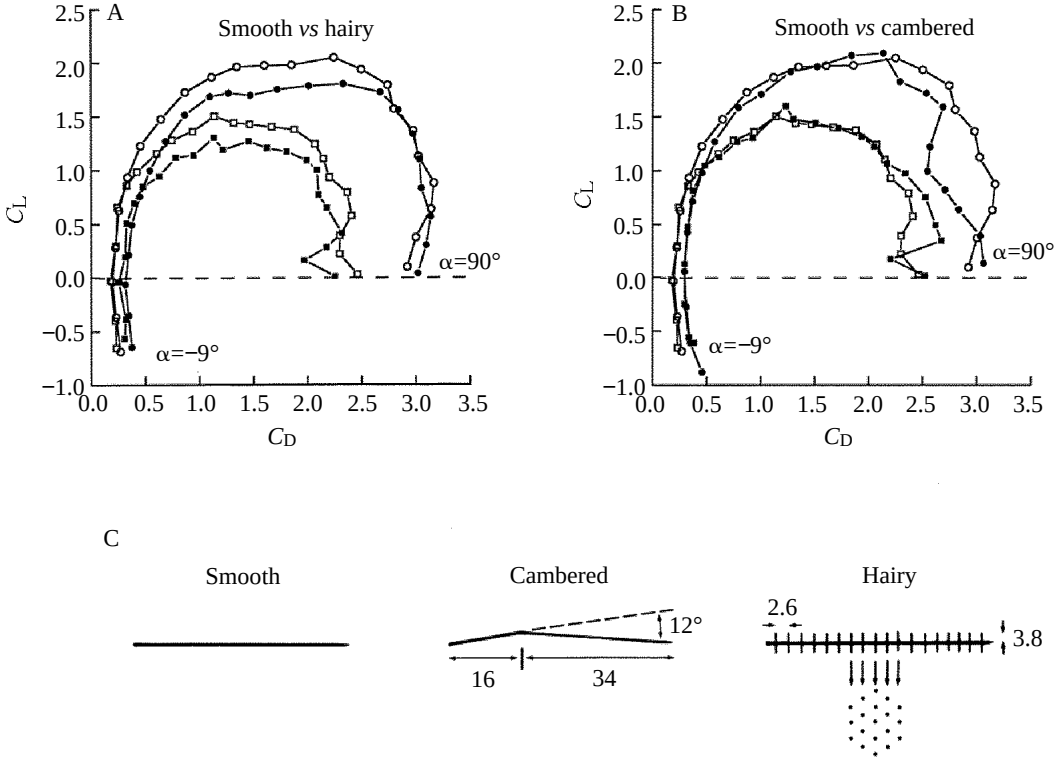

Fig. 7. Camber and increased surface roughness do not increase the performance of the wing model. Data for the smooth planar wing model in Fig. 4A (open symbols) are compared to data from the hairy profile (A) and the cambered profile (B). The Reynolds numbers for smooth, hairy and cambered profiles were 192, 185 and 197, respectively. Data after 2 chord lengths are shown by circles, and after 7 chord lengths by squares. The addition of fine projections on the wing increased C_D and decreased C_L at both early and late positions. The addition of camber to the profile had little effect on the aerodynamic performance, except for a slight increase in drag and greater instability at high angles of attack. Two-dimensional sections of the three experimental wing profiles (smooth, cambered and hairy) are shown in C. The 'tricombs' on the hairy profile consisted of aluminium staples glued in the hexagonal pattern indicated below the wing section. Measurements are given in millimetres.

development of transient vortex formation around the leading edge of the wing. As the Reynolds number increases, the ability of the wing to initiate the formation of the leading edge vortex is enhanced.

The effect of Reynolds number on the measured values of C_D late in translation also provides a useful test of the two-dimensional nature of the flow around the model wings. Fig. 6 plots the values C_D of at 0˚ and 90˚ angles of attack as a function of Reynolds number. The C_D values measured parallel to flow (open circles) closely match the relationship in equation 4, which considers only the contribution of skin friction. The C_D values of the plate normal to flow (filled circles) fit well the predictions of equation 5 for fully separated flow on a wing of infinite span (Ellington, 1991). Thus, the forces

generated by translation of the model wing are well approximated by the assumptions of two-dimensional flow.

Effects of surface roughness and camber on force coefficients

In earlier studies of *Drosophila* wing performance, Vogel (1967) noted that real wings exhibited a broad stall plateau that was not present in model wings, and he suggested that the behavior might be attributed to the rough surface of tricomb hairs. Further, he noted that cambering of both real and model wings greatly enhanced lift at positive angles of attack. We examined the effects of these two parameters on the performance of the two-dimensional profiles (Fig. 7). The absence of a sharp stall, already exhibited by the smooth profiles, was not enhanced by increased surface roughness, produced by glueing a hexagonal array of fine staples to the surface of the wing (see Fig. 7C). Rather, the presence of the staples caused a significant decrease in lift and increase in drag at both the early and late time points of translation (Fig. 7A). The increase in drag probably resulted from an elevation of skin friction caused by the additional surface area of the staples. Further, the addition of wing camber produced by bending the profile by 12˚ about a point 0.3 chords from the leading edge did not significantly alter aerodynamic performance (Fig. 7B), except for a slight increase in drag and greater instability at high angles of attack. Thus, we conclude that the broad lift plateau results from a property of thin airfoils at low Reynolds numbers and is not a product of morphological specializations. Nachtigall (1977) reached similar conclusions in studies of *Tipula* wings at a Reynolds number of 1500.

Discussion

The Wagner effect and delayed stall

The analysis of force production in wings impulsively started from rest began with Wagner's classic theoretical analysis, which predicted a slow development of circulation over the first several chord lengths of travel. The development of lift is similarly sluggish, although the wing instantaneously attains 50% of its steady-state value at the start of motion. These predictions were confirmed in elegant experiments by Walker (1931) using a conventional profile (RAF 130) at a Reynolds number of 140000. In accordance with these findings, we expected to find a sluggish development of lift at angles of attack below stall. We observed instead that lift on the thin wing model developed quickly towards steady-state values. The cause of this discrepancy is unclear, but the assumptions of zero viscosity inherent in the calculations of Wagner (1925) and well met in the measurements of Walker (1931), are certainly less appropriate in the range of Reynolds numbers used in these studies. In any event, it would not appear as if the delay in the generation of lift is of significance in the flight of small insects, especially compared to the great augmentation accrued at higher angles of attack discussed below.

Using the same experimental apparatus constructed by Walker, Francis and Cohen (1933) studied the development of circulation and lift at a 27.5˚ angle of attack, which is well above steady-state stall. They found that the circulation coefficient measured during the first few chords of travel was 50% higher than the predicted final value. The results

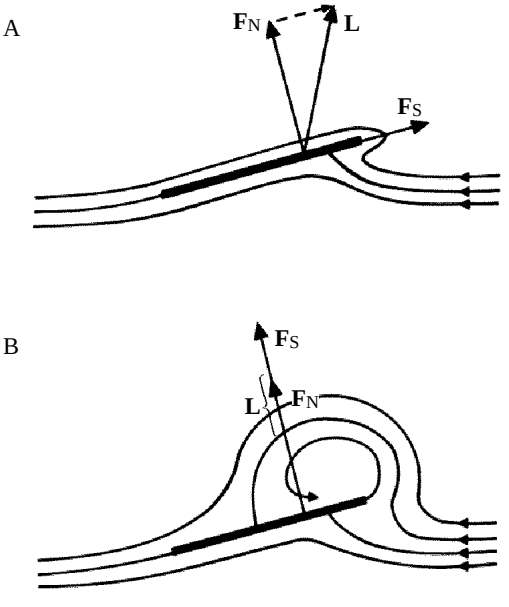

Fig. 8. The generation of detached vortex lift by rotation of leading edge suction vector on thin wings. (A) Conventional steady-state lift results from potential flow around a wing section and the Kutta condition on the trailing edge. The rapid change in velocity around a sharp leading edge results in a suction vector ($\mathbf{F}_S$) that acts parallel to the chord and sums with the normal force ($\mathbf{F}_N$) to produce the total lift ($\mathbf{L}$). (B) With the development of a leading edge vortex, a 'Kutta-like' condition replaces the rapid change in velocity around the leading edge, eliminating the parallel suction force. However, a suction force is now required to maintain the new attachment site on the upper surface, which adds directly with the normal force to generate a large increase in total lift. Thus, the change in pressure distribution resulting from the leading edge vortex is analogous to a 90° rotation of the leading edge suction vector.

reported here confirm that the mechanism of delayed stall could indeed provide a useful augmentation of lift in the range of Reynolds numbers relevant for the flight of *Drosophila*. At angles of attack greater than 13.5° the measured lift coefficients of the wing models were up to 80% higher after 2 chord lengths of travel, compared to the values measured 5 chord lengths later. Comparison of the force measurements with simultaneous flow visualization indicated that the transient peak in C_L correlates with the presence of a leading edge vortex that forms rapidly upon motion at large angles of attack and remains attached to the upper surface for the first few chord lengths of travel. The size of this vortex is much greater than the stable separation bubbles visualized in previous studies of real and model insect wings (Rees, 1975; Newman *et al.* 1977).

The generation of the vortex street

Despite the similarities with experiments at higher Reynolds numbers, the stall we observed in these model fly wings was not a static phenomenon. Thus, the analogy with the phenomenon of delayed stall may not be an appropriate model for the transient lift enhancement in this instance. In contrast to earlier studies of model *Drosophila* wings

(Vogel, 1967; and see below), we found that the flat wings generate a von Karman street for at least the first 7.5 chord lengths of travel. Although our experimental apparatus was only capable of this limited excursion, the oscillations of the force coefficients following the inertial transients are similar to the discrete vortex theory predictions for a flat plate (Sarpkaya, 1975; Fig. 8) and a conventional airfoil (Katz, 1981, Fig. 5) as well as actual flow patterns at a Reynolds numbers of 1050 (Kiya and Arie, 1977; Figs 4–6). As in both theoretical predictions, the amplitudes of oscillations in C_L and C_D are greatest in the first shedding cycle and subsequently decay asymptotically towards a steady-state level. The structure of oscillatory flows is characterized by the Strouhal number (*St*), which for airfoils is defined as $fc\sin\alpha/U$ (Katz, 1981); where f is the temporal frequency of vortex shedding and c is the chord length. Such a calculation made from the force trajectory data (Fig. 3A), yields a Strouhal number of approximately 0.14, which is in close agreement with other experimental measures for inclined flat plates (Fage and Johansen, 1927; Roshko, 1954), as well as the theoretical predictions mentioned above. The importance of this oscillatory structure on force production in insects may be assessed by considering the quantity $St\Lambda$, the Strouhal number times the mean number of chords travelled, which gives an estimate of the number of oscillations expected throughout a half-stroke. Using the equations of Ellington (1984*b*) and a 135° stroke plane in *Drosophila* (Zanker, 1990), the Λ value for a fruitfly is 1.7 chord lengths, corresponding approximately to the point of maximum force observed in these studies. Thus, the value of $St\Lambda$ would be 0.24, suggesting that the oscillations in the force coefficients generated by the von Karman pattern would not strongly influence the flight aerodynamics after the first half-cycle. However, the wing tip travels several more chord lengths than the base and, thus, the three-dimensional flow structure is likely to be more complex and could be influenced by the vortices generated after the first oscillation cycle.

How does the first large leading edge vortex enhance lift production over that expected under steady-state conditions? Previous authors (Rees, 1975; Newman *et al.* 1977; Maxworthy, 1979) have suggested that attached bubbles on insects wings might function by greatly enlarging the effective camber of the wing, and thus increase the production of conventional *potential lift*, which results from potential flow around the airfoil and application of the Kutta condition at the trailing edge. The Kutta condition is the empirically observed smooth tangential flow from the trailing edge of a wing in motion. A unique value of circulation, and thus lift, is required to maintain this condition at the trailing edge. In addition to the increase in potential lift by increased effective camber, a second framework has been useful for analyzing the augmentation of performance caused by leading edge vortices: *detached vortex lift* (Küchemann, 1978; Keuthe and Chow, 1986; Wu *et al.* 1992). Detached vortex lift results from the effect of a large leading edge vortex on the pressure distribution over the lifting surface of the wing and is utilized by thin delta-wing aircraft such as the *Concorde* and smaller military combat planes. The mechanisms underlying detached vortex lift have been elegantly analyzed by Polhamus (1971). In a thin airfoil without separation, a large leading edge suction force results from the enormous change in velocity required for flow around the leading edge (Fig. 8A). With the formation of the leading edge vortex, this suction is eliminated by the establishment of a Kutta-like condition on the leading edge. However, a normal suction

force is now required to maintain an attachment point of the vortex on the upper surface of the airfoil (Fig. 8B). Thus, the lift increase can be interpreted as a 90˚ rotation of the leading edge suction vector caused by the establishment of a stagnation point aft of the vortex. In the presence of a leading edge vortex, the suction vector is oriented normal to the surface of the wing and adds directly to the conventional lift component generated by potential flow. This interpretation for the augmentation of lift in fly wings seems preferable, in the case of the *Drosophila* wings, to the increased camber model, given that the size and structure of the large leading edge vortices produced by our wing model are analogous to those seen on vortex lift aircraft. Maxworthy (1979; footnote, page 61) has previously recognized this similarity, in noting that the three-dimensional flow induced by large leading edge vortices in his physical model of the fling behavior were somewhat analogous to those on delta-wing aircraft.

However, both theoretical frameworks used for analyzing detached vortices on airfoils, effective camber increase and detached vortex lift, were developed to explain steady-state conditions. The small vortices bound in wing corrugations are stable and produce a constant increase in effective camber (Rees, 1975; Newman *et al.* 1977). In the case of delta-wing aircraft, the large leading edge vortex is stable because of the presence of constant axial flow through the vortex center. Thus, the corrugations of insect wings and the axial flow on delta-wing aircraft are analogous in that they stabilize vortices on the lifting surface. Wu *et al.* (1992) have recently reviewed a number of additional mechanisms in airfoil design that enhance lift production through the stabilization of detached vortices. In contrast, the flows on the two-dimensional wing model started from rest are unsteady, and the performance of the wing eventually decays as the leading edge vortex is shed. However, lift augmentation by detached vortex lift may still be crucial for insect flight for two reasons. First, by analogy with delta wings, the leading edge vortex on actual insect wings might be stabilized by the presence of axial flow. Just such a mechanism was seen by Maxworthy (1979) in his three-dimensional modelling studies of the fling motion. Second, and perhaps more important, is the previous calculation that owing to the short translation distance only about one quarter cycle of von Karman shedding is encountered by the wing during each half-stroke. The limited translation distance of the wing stroke enables the fly to reap the benefits of increased lift from the temporary presence of a leading edge vortex, even though the flow is not stable over many chord lengths of translation. This strategy of exploiting the benefits of unstable leading edge bubbles over a short wing stroke was previously proposed by Ellington (1984*b*) in his discussion of delayed stall.

Comparisons with previous measures of Drosophila *wing aerodynamics*

In his classic analysis of *Drosophila* wing aerodynamics, Vogel (1967) reported that real fly wings and thin plate wing models differed substantially in their stall characteristics. He suggested that morphological specializations, such as the presence of wing tricombs, might be responsible for the absence of sharp stall on real wings. Further, Vogel reported that wing camber of thin plate models could augment lift by 25%. Our measurements on *Drosophila* wing models are in conflict with his results in several respects. First, our aerodynamic polar plots are quantitatively different from Vogel's

measurements for both his flat plate model and real fly wings. We measured significantly lower values of C_D and higher values of C_L at both the 2 and 7 chord points in translation. Such discrepancies might easily come from the rather different methods that were employed. In particular, the use of edge baffles in our apparatus limited induced drag resulting from spanwise flow. This interpretation is supported by the close agreement between the measured values of C_D at 0˚ and 90˚ angles of attack with the predictions based on two-dimensional flow (Fig. 6).

In addition to these quantitative differences, the performance of our flat plate models are qualitatively different from Vogel's in several respects. Even after 7 chords of travel, our profiles exhibited the same broad lift plateau that Vogel found in actual fly wings but not in flat plate models. Consistent with the fact that our simple models show the characteristics of Vogel's real fly wings, we detected no further increase in the aerodynamic performance of either cambered or 'hairy' profiles. As discussed earlier, the performance of our flat plate models after 7 chords of travel exhibited characteristics typical of *thin-airfoil stall*: a stutter in the development of lift at low angles of attack and the absence of a precipitous decline at higher angles. In contrast, the sharper stall in Vogel's data for flat plate model (Vogel, 1967, Fig. 3) is more characteristic of *leading edge stall*, resulting from an abrupt separation without subsequent reattachment. Finally, our measurements of an enormous augmentation of lift early in translation contradict Vogel's suggestion that the performance of wings that already avoid stall in the steady-state cannot be further enhanced by lift hysteresis or other unsteady mechanisms.

It is not likely that the above discrepancies are due to differences in Reynolds number, since both studies examined almost precisely the same range. The most likely cause lies in the unsteady nature of the flows that we observed. If the alternating vortical flow within this Reynolds number range and geometry are stable, then steady-state lift and drag measurements, such as those made by Vogel, actually record a time average of oscillating forces. However, Vogel found no evidence for the presence of von Karman trails in his studies, but instead reported the presence of stable bound vortices at high angles of attack. Therefore, another possible source of the discrepancy might be that the alternating pattern of vortex generation decays with sufficient time. Unfortunately, owing to the limited excursion of our apparatus, we could not determine whether the von Karman street initiated by our model at the start of translation would continue indefinitely or would eventually decay towards the steady-state pattern of stable bound vortices seen by Vogel. However, if such a decay over longer translation distances occurred, it would serve to emphasize the difficulty of interpreting the forces generated by flapping insect wings based on steady-state measurements.

The effect of Reynolds number on unsteady mechanisms of lift production

The size of the lift augmentation present during the first chord lengths of movement decreases as the Reynolds number is lowered from about 230 to 75. This trend is significant in two ways. First, the same approximate Reynolds number gradient is found by moving from the distal tip of the wing towards the base, owing to the change in translational velocity (see Zanker, 1990). This implies that the three-dimensional flow pattern of the wing could be quite complex and that distal portions could contribute

proportionally more to lift as a result of a larger leading edge vortex in that region. As stated earlier, however, interpretation of the two-dimensional results is complicated by the fact that the distal tip could translate through several cycles of alternating vortex generation. Nevertheless, the leading edge vortex on real wings is likely to be greatly stabilized by axial flow. Given these effects and the gradient of velocity and stroke distance along the wing, the three-dimensional flows of actual wings during flight are not easy to predict. The complex nature of the actual flows can be appreciated from Maxworthy's (1979) reconstruction of the three-dimensional flow structure of leading edge vortices generated during the fling behavior.

Second, forgetting momentarily the velocity gradient along the wing, and considering instead mean values of wing size and wing beat frequency, the 75–230 Reynolds number range encompasses a broad assemblage of species within the diverse drosophilid radiation. As argued above, flies might exploit the large augmentation of wing performance generated by detached vortex lift during their short wing stroke. However, as is clear from Fig. 5A, the magnitude of the lift augmentation that is available by this unsteady mechanism decays with decreasing Reynolds number. Thus, closely related flies that differ in size but presumably utilize virtually identical musculature and flight control circuitry may not be capable of exploiting identical aerodynamic mechanisms. In the future, it will be of interest to determine whether the radiation of different-sized species within this critical fluid dynamic range has enforced a significant alteration in the kinematics *via* changes in morphology and the neuromuscular control of flight.

Relevance of physical models to real wing kinematics

The patterns of wing movements in insects, particularly among the highly maneuverable flies, are among the most complex and rapidly controlled of any locomotory appendage. Can a motion as simple as that described here, translation from rest to a fixed velocity, offer any insight into the mechanisms of force production in real flies? If nothing else, the results of these model studies suggest that the flows relevant in the flight of small insect are unsteady and that conclusions based on steady-state measures could greatly underestimate the performance of flapping wings. At low Reynolds numbers, the development of lift, rather than being significantly delayed by the Wagner effect, can be greatly augmented by the production of large leading edge vortices. The lift coefficients measured under these conditions are much greater than those reported for any insect wing or wing model at steady state. Further, although the motions of the two-dimensional profiles are simple, they do serve as reasonable models of certain aspects of the actual wing motion. In detailed kinematic measures of tethered flight in *Drosophila*, Zanker (1990) found that the motion of the wings in the horizontal plane during flight is distinctly sawtooth in form and is, thus, relatively well approximated by reciprocating movements at constant velocity. In addition, the instantaneous aerodynamic angle of attack is stable throughout most of the downstroke at a value well above that required for unsteady flow in these experiments (Zanker and Götz, 1990). The fly also maintains a large and nearly constant negative angle of attack during the upstroke. Perhaps the most abstract simplification of our physical model is the absence of wing rotation. Although the aerodynamic angle of attack is relatively stable during the two half-strokes, the

angular velocity of the wings during stroke reversal is large and can exceed 10^5 degrees s^{-1} during the transition from downstroke to upstroke. However, in experiments that will be reported in a forthcoming paper we have found that the addition of wing rotation at the onset of translation does not alter the general conclusions presented here, although such motion can result in an even larger enhancement of lift.

We wish to thank Fritz Olaf-Lehman and Roland Strauss for intellectual and technical support during the execution of this work. The project was funded by the Max-Planck Gesellschaft.

References

BENNETT, L. (1977). Clap and fling aerodynamics – an experimental evaluation. *J. exp. Biol.* **69**, 261–272.

DUDLEY, R. AND ELLINGTON, C. P. (1990). Mechanics of forward flight in bumblebees. II. Quasi-steady lift and power requirements. *J. exp. Biol.* **148**, 53–88.

ELLINGTON, C. P. (1975). Non-steady-state aerodynamics of the flight of *Encarsia formosa*. In *Swimming and Flying in Nature* (ed. T. Y. Wu, C. J. Brokaw and C. Brennen), vol. 2, pp. 783–796. New York: Plenum Press.

ELLINGTON, C. P. (1980). Vortices and hovering flight. In *Instationäre Effekte an Schwingenden Tierflügeln* (ed. W. Nachtigall), pp. 64–101. Wiesbaden: Franz Stiener.

ELLINGTON, C. P.(1984*a*). The aerodynamics of hovering insect flight. I. The quasi-steady analysis. *Phil. Trans. R. Soc. Lond. B* **305**, 1–15.

ELLINGTON, C. P. (1984*b*). The aerodynamics of hovering insect flight. IV. Aerodynamic mechanisms. *Phil. Trans. R. Soc. Lond. B* **305**, 79–113.

ELLINGTON, C. P. (1991). Aerodynamics and the origin of flight. *Adv. Insect Physiol.* **23**, 171–210.

ENNOS, A. R. (1989). The kinematics and aerodynamics of the free flight of some Diptera. *J. exp. Biol.* **142**, 49–85.

FAGE, A. AND JOHANSEN, F. C. (1927). On the flow of air behind an inclined flat plate of infinite span. *R. & M.* No. **1104**, British ARC (*Proc. R. Soc. Lond. A* **116**, 170).

FRANCIS, R. H. AND COHEN, J. (1933). The flow near a wing which starts suddenly from rest and then stalls. *Rep. Memo. aeronaut. Res. Comm. no.* **1561**.

GÖTZ, K. G. (1987). Course-control, metabolism and wing interference during ultralong tethered flight in *Drosophila melanogaster*. *J. exp. Biol.* **128**, 35–46.

JENSEN, M. (1956). Biology and physics of locust flight. III. The aerodynamics of locust flight. *Phil. Trans. R. Soc Lond. B* **239**, 511–552.

KATZ, J. (1981). A discrete vortex method for non-steady separated flow over an airfoil. *J. Fluid Mech.* **102**, 315–328.

KEUTHE, A. M. AND CHOW, C.(1986). *Foundations of Aerodynamics.* New York: John Wiley.

KIYA, M. AND ARIE, M. (1977). A contribution to an inviscid vortex-shedding model for an inclined flat plate in uniform flow. *J. Fluid Mech.* **82**, 223–240.

KÜCHEMANN, D. (1978). *The Design of Aircraft.* Oxford, Pergamon.

LIGHTHILL, M. J. (1973). On the Weis-Fogh mechanism of lift generation. *J. Fluid Mech.* **60**, 1–17.

MARMARELIS, P. Z. AND MARMARELIS, V. Z.(1978). *Analysis of Physiological Systems: The White Noise Approach*. New York: Plenum Press.

MAXWORTHY, T. (1979). Experiments on the Weis-Fogh mechanism of lift generation by insects in hovering flight. I. Dynamics of the fling. *J. Fluid Mech.* **93**, 47–63.

MAXWORTHY, T. (1981). The fluid dynamics of insect flight. *A. Rev. Fluid Mech.* **13**, 329–350.

MCCOLLOUGH, G. B. AND GALT, D. E. (1951). Examples of three representative types of airfoil-section stall at low speed. *Tech. Notes nat. advis. Comm. Aeronaut. Washington* no. **2502**.

NACHTIGALL, W. (1977). Die aerodynamische Polare des Tipula-Flugels und eine Einrichtung zur halbautomatischen Polarenaufnahme. *Fortschr. Zool.* **24**, 347–352.

NACHTIGALL, W. (1979). Rasche Richtungsänderungen und Torsionen schwingender Fliegenflügel und Hypothesen über zugeordnete instationäre Strömungseffekte. *J. comp. Physiol.* **133**, 351–355.

NEWMAN, B. G., SAVAGE, S. B. AND SCHOUELLA, D.(1977). Model tests on a wing section of an *Aeschna* dragonfly. In *Scale Effects in Animal Locomotion.* (ed. T. J. Pedley), pp. 445–477. London: Academic Press.

POLHAMUS, E. C. (1971). Predictions of vortex lift characteristics by a leading-edge suction analogy. *J. Aircraft* **8**, 193–198.

REES, C. J. C. (1975). Aerodynamic properties of an insect wing section and a smooth aerfoil compared. *Nature* **258**, 141–142.

ROSHKO, A. (1954). On drag and shedding frequency of two-dimensional bluff bodies. *N.A.C.A.* Tech. Note No. 3169.

SARPKAYA, T. (1975). An inviscid model of two-dimensional vortex shedding for transient and asymptotically steady separated flow over an inclined plane. *J. Fluid Mech.* **68**, 109–128.

SAVAGE, S. B., NEWMAN, B. G. AND WONG, D. T.-M. (1979). The role of vortices and unsteady effects during the hovering flight of dragonflies. *J. exp. Biol.* **83**, 59–77.

SCHLICHTING, H.(1979). *Boundary-Layer Theory.* New York: McGraw Hill.

SOMPS, C. AND LUTTGES, M. (1985). Dragonfly flight: novel uses of unsteady separated flows. *Science* **228**, 1326–1329.

SPEDDING, G. R. AND MAXWORTHY, T. (1986). The generation of circulation and lift in a rigid two-dimensional fling. *J. Fluid Mech.* **165**, 247–272.

TANI, I.(1964). Low-speed flows involving bubble separations. *Prog. aeronaut. Sci.* **5**, 70–103.

TIETZE, U. AND SCHENK, C.(1990). *Electronic Circuits.* Berlin: Springer-Verlag.

VOGEL, S.(1967). Flight in *Drosophila*. III. Aerodynamic characteristics of fly wings and wing models. *J. exp. Biol.* **44**, 431–443.

VOGEL, S.(1981). *Life in Moving Fluids.* Princeton: Princeton Univerity Press.

WAGNER, H. (1925). Über die Entstehung des dynamischen Auftriebes von Tragflügeln. *Z. agnew. Mat. Mech.* **5**, 17–35.

WALKER, P. B.(1931). Growth of circulation about a wing and an apparatus for measuring fluid motion. *Reports and Mem., Aeronaut. Res. Com.* no. **1402**.

WEIS-FOGH, T. (1973). Quick estimates of flight fitness in hovering animals, including novel mechanisms for lift production. *J. exp. Biol.* **59**, 169–230.

WU, J. Z., VAKILI, A. D. AND WU, J. M. (1992). Review of physics of enhancing vortex lift by unsteady excitation. *Prog. Aerospace Sci.* **28**, 73–131.

ZANKER, J. M. (1990). The wing beat of *Drosophila melanogaster.* I. Kinematics. *Phil. Trans. R. Soc. Lond. B* **327**, 1–8.

ZANKER, J. M. AND GÖTZ, K. (1990). The wing beat of *Drosophila melanogaster.* II. Dynamics. *Phil. Trans. R. Soc. Lond. B* **327**, 19–44.

Figure 3 – Colour

Fig. 3